Fracture mechanisms of additively manufactured polylactide: effect of in vitro hydrolytic degradation

Amirpasha Moetazedian, Andrew Gleadall* and Vadim V Silberschmidt

Wolfson School of Mechanical, Electrical and Manufacturing Engineering, Loughborough University, Loughborough, LE11 3TU, UK

*Corresponding author – Email: A.Gleadall@lboro.ac.uk; Tel: +44 (0) 1509 227578

Graphical abstract

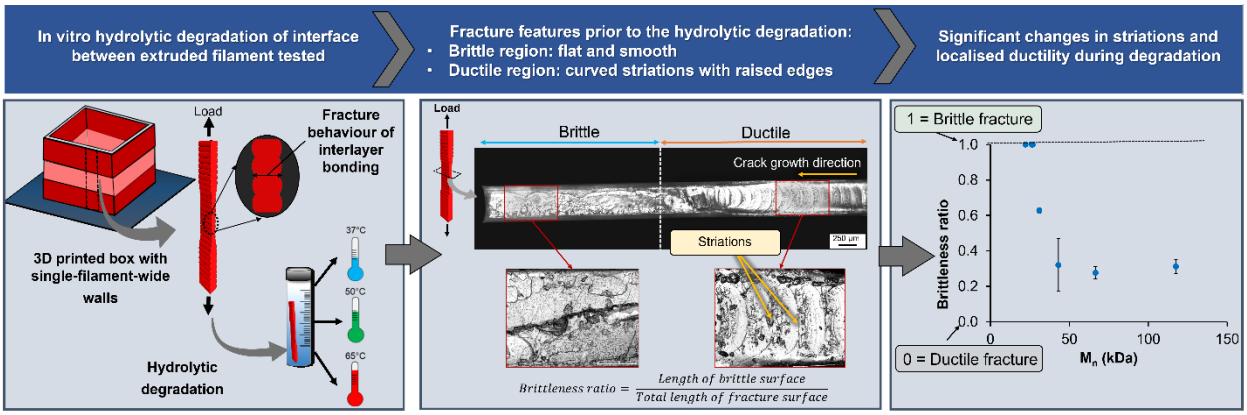

Abstract

This is the first study considering the effect of in vitro hydrolytic degradation at 37ºC on fracture mechanism of the most important aspect of additive manufacturing – the interface between layers. Specimens were tested transversely (failure between layers) and longitudinally (failure directly through extruded filaments) under testing conditions similar to those in the human body (submerged at 37°C). Feature of fracture surface, including striations and localised ductility, significantly changed when degradation caused a reduction in molecular weight below 40 kDa from the initial 240 kDa or an increase in crystallinity above 12%. Such changes indicated a transition from more ductile to more brittle fracture during degradation.

Keywords: Additive manufacturing; Fracture; Degradation; Crystallinity; Molecular weight

1 Introduction

Synthetic biodegradable polymers are extensively used in biomedical applications as they offer many desirable properties including the capability to tailor degradation kinetics and mechanical properties for a specific application [1], [2]. Amongst them, polylactide (PLA) is one of the most studied polymers thanks to its higher strength and better processability compared to other polymers [3]. For biomedical applications, PLA demonstrates excellent biocompatibility, and its degradation products can be metabolised and secreted by the human body. This makes it a compelling candidate for a wide range of applications including bioresorbable stents, orthopaedic fixation plates, screws, tissue-engineering scaffolds and drug-delivery devices [2]–[8].

Fabrication of PLA components with material extrusion additive manufacturing (MEAM) – also referred to as *fused filament fabrication (FFF)* and *fused deposition modelling (FDM)* – has grown significantly, as the process transitions from a prototyping technology to a true manufacturing technology that produces intricate and customised structures, such as patient-specific medical implants. MEAM works by deposition of molten polymer through a hot nozzle that moves across the print platform (in the X-Y planes), while the print platform gradually moves down (in the Z direction) to build the part layer-by-layer. This layer-wise nature of the process is historically considered as the source of anisotropy due to “poor interlayer bonding between filaments” in the Z direction. In the last few years, the fracture and damage of additively manufactured biomedical implants have been researched extensively in healthcare engineering, thus gathering considerable attention from specialists in mechanics of materials and fracture. Studies by the authors [9], [10] implemented a novel and simple method (specifically, single-filament-wide specimens as opposed to the ASTM standard specimen geometry with non-standardised and complex print paths) to gain fundamental understanding of mechanical performance of 3D-printed PLA. The lack of understanding of mechanical behaviour during degradation, including fracture mechanisms, is a crucial question that needs to be answered.

For this purpose, in a recent study by the authors [11], the in vitro hydrolytic degradation of additively manufactured PLA at 37ºC was considered, and it was found that the interlayer interface was stable and degraded in a manner similar to that of the bulk material. Furthermore, fracture surfaces of degraded specimens showed

interesting features, which appeared to change with degradation time. This research [11] gives important confidence in the use of 3D printed PLA for bioresorbable medical devices but highlights the need to further investigate the fracture mechanisms. In the literature, there is a limited attention towards fracture analysis of 3D printed PLA during in vitro hydrolytic degradation. For example, a study by Gonzalez Ausejo et al. [12] considered hydrolytic degradation of 3D printed PLA in two directions: normal to (Z-direction), and along the print platform (XY-plane) at 50ºC and 70ºC. In the same study, authors highlighted that *"vertical specimens showed a smooth [fracture] surface, and the horizontal specimens exhibit an irregular surface"* but did not investigate further. More importantly, there is no study which relates such features to the microstructural changes during in vitro hydrolytic degradation (for instance, crystallinity, molecular weight (M_w) and mechanical properties). Herein, for the first time, the effect of in vitro hydrolytic degradation at body temperature on the fracture mechanisms of the additively manufactured PLA in terms of crack initiation and growth is studied. Previously validated micro-tensile specimens [9] were used to precisely characterise fracture surfaces before and after a range of degradation durations. The applicability of results and suitability of accelerated temperature to predict failure mechanisms at body temperature were also discussed.

2 Materials and methods

This section outlines the materials and the manufacturing process of specimens followed by descriptions of characterisation methods.

2.1 Materials

Natural PLA filament (3DXTECH® branded NatureWorks® polylactide 4043D, Sigma Aldrich) with a density of 1.25 $g.cm^{-3}$ was used in this study. The chemical properties of raw filament in terms of weight average molecular weight (M_w) and number average molecular weight (M_n) were measured as 240 kDa and 120 kDa, respectively. The ultimate tensile strength, tensile modulus and strain-at-fracture of the bulk material were 62.8 MPa, 2.65 GPa and 0.0507, respectively, when tested in standard laboratory conditions [10].

2.2 Specimen design and additive manufacturing

A RepRap x400 system with a 0.4-mm nozzle was used to deposit a hollow square made of single-filament PLA with dimensions of 45 mm (W) x 45 mm (H), at a constant extrusion temperature of 210ºC and printing speed of 1000 mm/min (see Table 1). The design (Figure 1a) was created using an in-house software ("Full Control GCode Designer" – available from www.fullcontrolgcode.com) to allow a full control over the print path, which was necessary and beneficial to produce this geometry as validated in our previous studies [9], [13], [14]. The extruded-filament width (EFW) and the layer height in the gauge region were 0.5 mm and 0.2 mm, respectively (Table 1). The design of specimens in this study was adapted from ASTM D1708 [15] and it was implemented at a scale of individual extruded filaments, which is the smallest possible building block for this process. This enabled precise characterisation of the interfacial bond by measuring the cross-sectional area, which is not possible for current ASTM standard tensile-testing specimens with complex, non-standardised print paths.

Table 1 *Printing parameters used to produce specimens.*

Printing parameters	**Value**
Nozzle diameter	0.4 mm
Nozzle temperature	210°C
Print platform temperature	60°C
Printing speed	1000 mm/min
Layer height	0.2 mm
Extruded-filament width in gauge region	0.5 mm

In this study, the effect of in vitro hydrolytic degradation on fracture behaviour of the best and worst orientation for additively manufactured specimens were considered: (i) the direction of extruded filament (denoted as F), representing the best possible printing orientation, to assess the bulk-material properties; (ii) normal to the interface between layers (denoted as Z), representing the worst possible orientation. Once all specimens were printed, custom tools with razor blades were used to cut the boxes into 5 mm-wide and 45 mm-tall dog-bone specimens without causing any negative edge-effects as validated before with respect to bulk-material properties [9], [10].

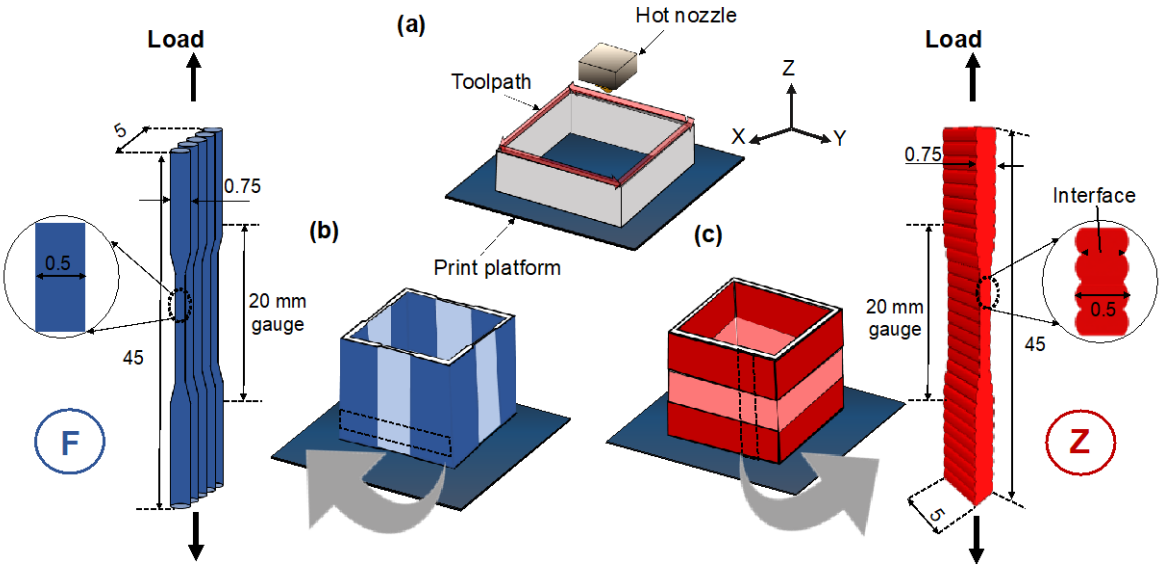

Figure 1 *(a) Toolpath used for generation of single-filament-wide walls in two testing directions: along the filament direction and parallel to the print platform (b) (denoted as F) and normal to the print platform (c) (denoted as Z). Testing direction is indicated by arrows. Dashed rectangles on the boxes represent the outline of cut specimens (all dimensions are in mm) [11].*

2.3 Hydrolytic degradation

The in vitro hydrolytic degradation of Z and F specimens were conducted at 37°C in an oven by placing specimens in 30 ml of phosphate buffer saline solution (PBS) with a neutral pH of 7.4 ± 0.2 according to ISO13781:2017 [16]. Hydrolytic degradation at elevated temperatures of 50°C and 65°C was also considered to compare the properties with those for degradation at body temperature (i.e., 37°C). The pH level of PBS solution was checked regularly and maintained within 7.4 ± 0.2 throughout the experiment by refreshing the media regularly (e.g., every 2 days for 65°C, every 10 days for 50°C and every 30 days for 37°C).

2.4 Characterisation

2.4.1 Tensile testing

Both Z and F specimens (n = 10 for each testing direction) were mechanically tested submerged at 37°C (replicating the human body) to prevent two-fold overestimation of properties when testing in air and at room temperature [9]. For this purpose, an Instron 5944 equipped with a BioPuls Bath system containing a temperature-controlled bath (Instron BioPuls, Instron, USA) was used. Since undegraded F-specimens did not fail when tested submerged at 37°C, they were also tested submerged at 20°C to produce

a fracture surface. Specimens were first placed in the bath for half an hour before starting the test to ensure uniform temperature and water absorption [9]. Hydrated specimens were subjected to uniaxial tension at a constant displacement rate of 0.5 mm/min (4 x 10^{-4} s^{-1} strain rate) using a 2 kN load cell. To ensure that the results were not affected by the load cell, F specimens were also tested using a 500 N load cell, and there was less than 1 MPa difference between the average strength values obtained with the two load cells. The pre-fracture cross-sectional area was used for strength calculation – measured using a Zeiss Primotech optical microscope. For Z specimens, the mean bond width was calculated from ten replicates to determine cross-sectional area. Meanwhile, for F specimens, the total cross-sectional area of filaments was measured [9].

2.4.2 Differential scanning calorimetry

The mean crystallinity of specimens from two replicates was determined using a TQ2000 (TA, instrument, USA) Differential Scanning Calorimetry (DSC) system. Approximately 10 mg of PLA from the gauge section was loaded onto the aluminium pans. Thermal analysis was started by heating the material from 20 to 200°C at a ramping rate of 10°C.min^{-1}. The degree of crystallinity (X_c %) was calculated as follows:

$$X_c = \frac{\Delta H_m - \Delta H_{cc}}{\Delta H^0{}_m} \times 100\% , \quad (3)$$

where ΔH_m, ΔH_{cc} and $\Delta H^0{}_m$ are melting enthalpy (J.g^{-1}), cold crystallisation enthalpy (J.g^{-1}) and enthalpy of fusion for 100% crystalline PLA, which is 93.1 J.g^{-1} [9], [17].

2.4.3 Gel permeation chromatography

The average M_w and M_n for both F and Z specimens (n = 2 for each testing direction) were measured against two replicates using a gel permeation chromatography (GPC) system (Infinity 1260, Agilent Technologies). A section of gauge region was dissolved in $CHCl_3$ + 2% triethylamine at a concentration of 1 mg/ml. The GPC solutions were left to dissolve for 2 days before transferring into a GPC vial via a syringe containing 0.22 µm filter. The GPC analysis was performed using a 100 µl injection volume at a flow rate of 1 ml.min^{-1} with a refractive index (RI) detector at 40°C using two Plgel mixed C columns. The data were examined using Cirrus SEC software against the polystyrene standards [18], [19].

2.4.4 Optical microscopy

The fracture surface of each specimen was examined using a Zeiss Primotech optical microscope at various magnifications. Alicona G4 InfiniteFocus (Bruker, Germany) was used to capture high-resolution 3D scans of the entire fracture surface at a 10× magnification for both specimen types before degradation. The scans were post-processed using Mountains Premium 7.4 software (Digital surf, France).

3 Results and discussion

This section is divided into the following sections:

- Section 3.1 – Understanding the fracture mechanisms of specimens in tensile tests in terms of crack initiation and direction of growth before degradation to identify the key features of the fracture surface.
- Section 3.2 – Analysing the changes in fracture-surface features of specimens during degradation at 37ºC and relating them to mechanical, chemical and thermal properties.
- Section 3.3 – Applicability of results and suitability of using elevated temperatures (50°C and 65°C) to predict failure mechanisms at body temperature.

3.1 Fracture mechanisms of specimens before in vitro hydrolytic degradation

To characterise fracture mechanisms before in vitro hydrolytic degradation, optical micrographs were taken for the entire fracture surfaces of undegraded Z and F specimens, as demonstrated in Figure 2. The 3D scan and surface profiles of these surfaces were discussed in more detail in a previous study [9], but the direction of extruded-filaments can be distinguished by the presence of smooth edges due to their orientation along the direction of fracture. In contrast, curved external surfaces (above/below, Figure 2) were seen for F specimens since fracture occurred directly through extruded filaments.

Examining the specimens during tensile tests (see Figure 3 for stress-strain curves) revealed that fracture behaviours of Z and F specimens differed. The former exhibited sudden fracture with a flat surface, whereas the latter demonstrated greater plasticity before failure with a rough fracture surface. The fracture path of Z specimen was along the interface between the printed layers, following the geometric stress concentrators (i.e. naturally occurring grooves between filaments on adjacent layers), which initiated the crack. Apparently, the plasticisation of polymer by water (submerged testing conditions) prevented the sudden failure – a typical failure for similar specimens tested

in air at room temperature [9]. Instead, plastic strain occurred after yielding with fluctuations in load (as apparent in stress-strain curves in Figure 3). From micrographs of fracture surfaces, it was evidenced the presence of two distinct areas across the fracture surfaces:

(i) a region combining both brittle and ductile surface features - i.e., a flat surface indicating the brittle fracture but with raised edges (apparent shear lips) and curved striations indicating the ductile fracture;

(ii) a region with a flat and smooth surface indicating the brittle fracture.

Based on micrographs and unpublished results of notched specimens, the crack started at the end with striations (right-hand side in Figure 2) during tensile tests. The striations likely formed due to quick propagation of a crack between crazes ahead of the crack tip, based on analysis done by Doyle et al. [20]. Once the crack reached a certain length, a faster brittle-crack propagation occurred, with sudden failure as indicated by the flat and smooth surface on the left-hand side in Figure 2. Micrographs of the brittle-ductile area at a higher magnification showed that the distance between these striations was on average 121.4 μm. Furthermore, a considerable change in the length of brittle and ductile areas was also identified during in vitro hydrolytic degradation. As a result, authors introduced a parameter termed *brittleness* by simply dividing the length of the brittle area (shown in Figure 2) by the total length of the fracture surface of specimens measured from optical micrographs (mean of five specimens). When the parameter approached 1, it indicated the brittle fracture as the predominant failure mode. Changes to these features during degradation are discussed shortly in Section 3.2.

For the F specimens, plasticisation of the material submerged in water at body temperature caused extensive plasticity. Strains of 40% were achieved without failure, making fractography impossible. Therefore, F specimens were also tested submerged at 20ºC to achieve an observable fracture surface and provide understanding of material behaviour that would not be possible for testing submerged at 37°C. The fracture of the F specimens was caused by propagation of the crack through multiple interlayer bonds with no apparent debonding even though there was a large plasticity prior to failure (mean strain-at-fracture was 16.5%).

The 3D scans and the extracted surface profiles showed apparent shear lips along both edges, which is a characteristic of ductile failure. This could further explain the

plastic deformation observed in the tensile tests. Furthermore, the vein-like patterns in the F-specimen's fracture surfaces were in fact internal necking (Figure 2). It is assumed that, when testing at 37°C, these regions of necking were able to extend across the entire specimen thickness, leading to extensive necking and no failure [9].

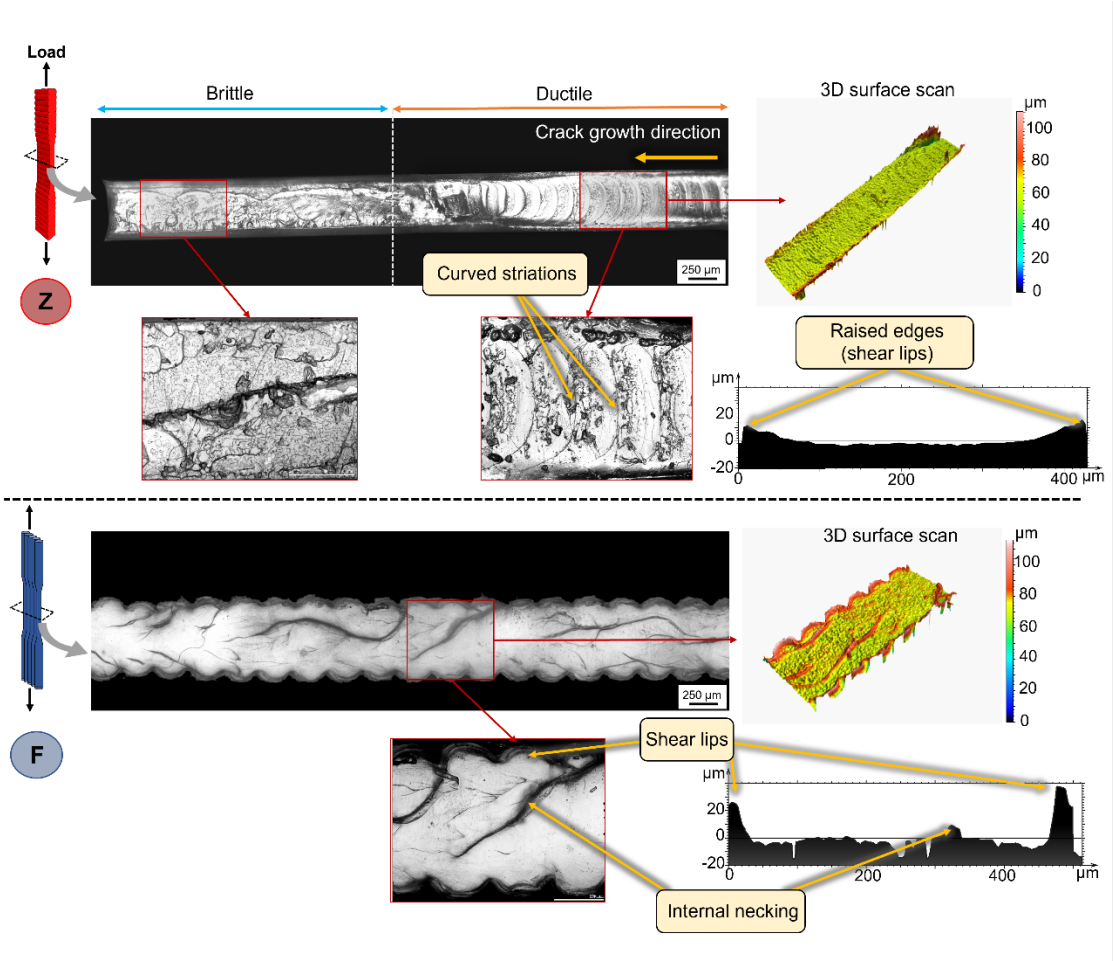

Figure 2 *Optical micrographs along with 3D-scans and surface profiles of fracture surfaces of Z (top row) and F (bottom row) specimens before degradation. Curved striations at one end of Z specimens indicated a transition from brittle to brittle-ductile fracture. Curved striations and shear lips were apparent in the fracture surface in the ductile region. F specimens strained by 40% without failure so fractography was not possible. Therefore, F specimens were also tested submerged at a lower temperature (20ºC) to achieve a fracture surface. There were larger shear lips than in Z specimens and internal necking occurred.*

3.2 Fracture mechanisms of specimens during in vitro hydrolytic degradation at 37ºC

This section discusses the changes observed in fracture features of specimens in during in vitro hydrolytic degradation at body temperature for up to 240 days. The representative stress-strain curves of Z and F specimens degraded at 37ºC, along with micrographs of fracture surfaces after mechanical tests, are shown in Figure 3. The results of tensile tests demonstrated that peak stress levels at day 0 for F and Z

specimens were very close (33.1 MPa and 27.5 MPa, respectively), indicating that the interfacial bond has properties similar to the bulk material [11].

As degradation continued, there was a slight increase in the tensile modulus as a result of increasing crystallinity (see our other study [11]). Such changes appeared to alter the features present across the fracture surfaces, resulting in a transition from a ductile-brittle fracture to brittle fracture. For example, the distance between curved striations gradually decreased during degradation, indicating that the material could accommodate less crazing ahead of the crack tip before the crack propagated. Furthermore, striations disappeared after 180 days due to the increase in crystallinity (discussed in relation to Figure 4), at which point the fracture surface was typical of brittle fracture – flat and smooth. The micrographs in Figure 3 clearly demonstrate that the in vitro degradation had a pronounced effect on the fracture of specimens in terms of crack propagation mechanisms and the resultant fracture surface features. These trends agree with the stress-strain curves, with apparent transitions in the overall failure mechanism from ductile to brittle.

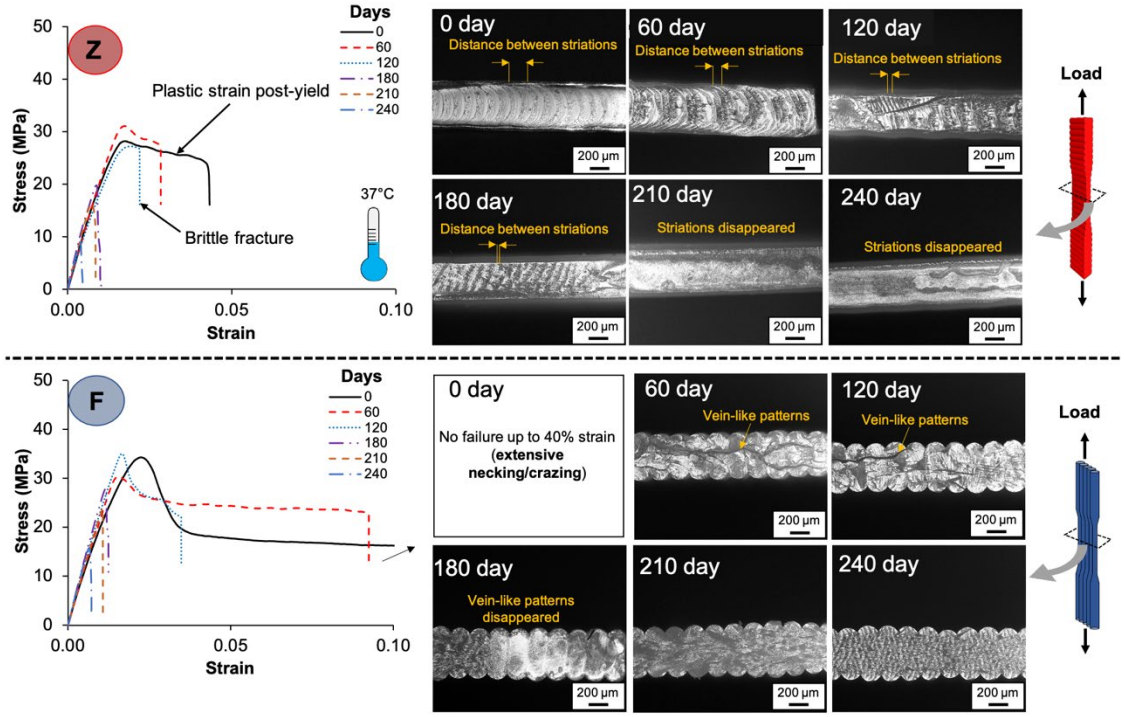

Figure 3 *Representative stress-strain curves and corresponding micrographs of fracture surfaces for Z (top row) and F (bottom row) specimens during hydrolytic degradation at 37ºC for different periods of time. Irrespective of testing directions, there was a transition from a ductile-brittle fracture to a brittle one manifested by disappearance of the curved striations (Z specimens) and necking (F specimens). The black arrow in F specimens indicates no failure for undegraded F specimens at tension up to 40% strain.*

The evolution of properties for Z specimens over time are shown in Figure 4. Apparently, M_n decreased over 240 days of degradation (Figure 4a), due to the random chains scissions as evaluated in our previous study [11]. The chain scissions provided enough mobility for shorter chains to form new crystalline regions, thus, the degree of crystallinity increased over time (Figure 4b). Such a change in the crystallinity was responsible for the reductions in both strain-at-fracture (Figure 4c) and toughness with time (Figure 4d). Analysing the evolution of fracture features with time indicated that the distance between striations showed a considerable reduction (48.1%) for the first 60 days; after it reduced by 22.5 μm for every 60 days until 180 days (Figure 4e), after which no striations were visible. The trend for the introduced brittleness parameter with increasing degradation time was the opposite, reaching the value of 1 after 210 days, confirming the brittle failure (i.e., increase in crystallinity). The trends for fracture surfaces possibly occurred due to the transition in fracture from ductile to brittle as a result of changes in M_n and crystallinity. To understand the effects of changes in M_n and crystallinity on fracture behaviour of PLA, the next section considers the relationship between fracture features and mechanical, thermal and chemical properties.

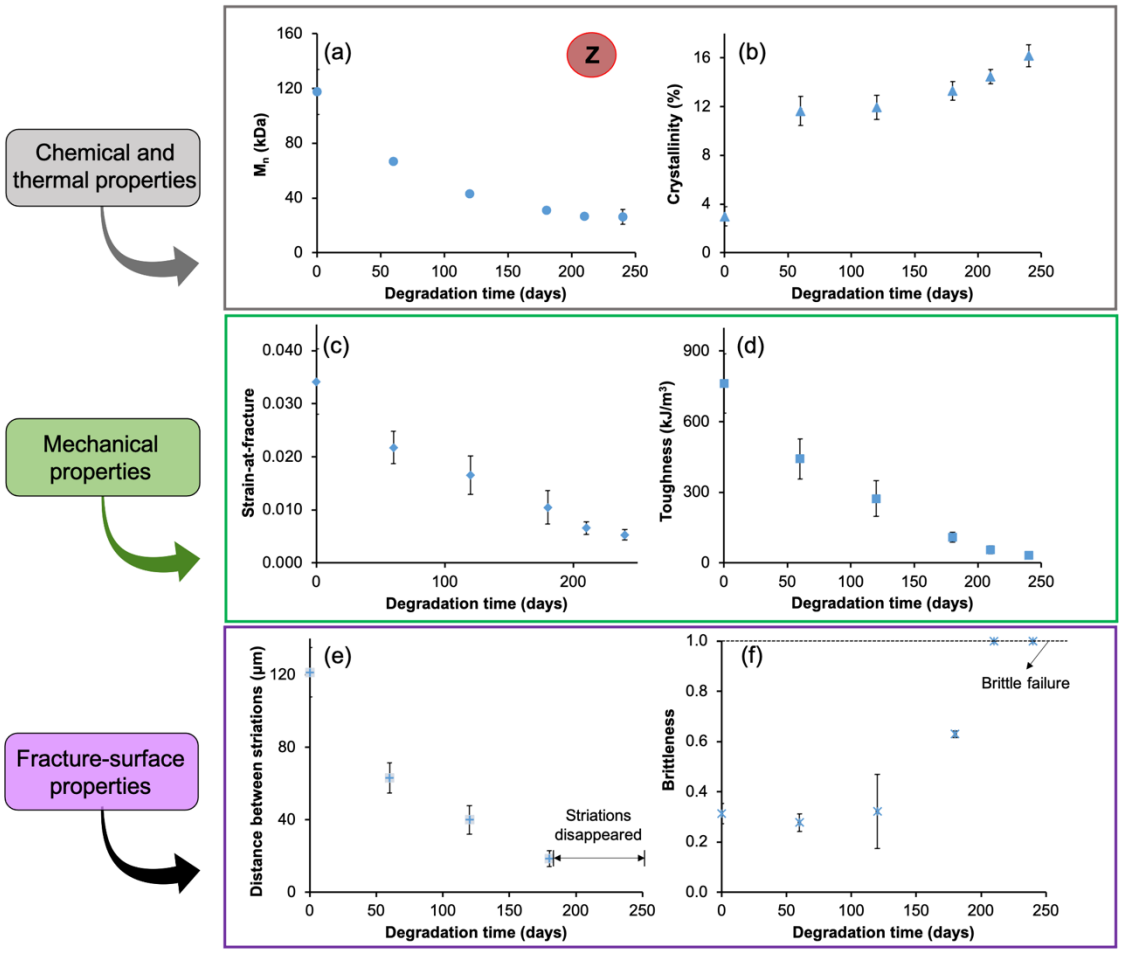

Figure 4 *Evolution of properties for Z specimens degraded at 37°C for 240 days: (a) degradation of M_n versus time; (b) increase in crystallinity; (c) reduction in both strain-at-fracture and (d) toughness (d); (e) reduction in normalised distance between striations; and (f) increase in brittleness parameter. Error bars indicate standard deviation.*

For further analyses, the sideview micrographs of specimens were used to study variation in cross-sectional thickness of 3D-printed specimens (Figure 5). For the undegraded Z specimens (0 day), a significant amount of deformation (necking) was apparent near the point of fracture. Such extensive deformation prior to failure (40.1% reduction in width) confirmed that the material fully yielded and highlighted that the interlayer bond was not particularly weak (as often reported) since it was able to sustain forces that generated extensive plastic deformation of the bulk material. Such observation gives further confidence in disproving the ideas about deficiencies in interlayer bond strength as detailed in other recent studies [9]–[11], [21]. The sideview micrographs of the degraded Z specimens showed magnitude of local plastic deformation and necking reduced after 120 days (and even further reduced after 210 days), indicating a transition from a more ductile material to a more brittle one.

Moreover, thickness of the degraded specimens demonstrated no reduction in EFWs as result of a brittle fracture due to rapid crack propagation as opposed to ductile fracture.

For the F specimens, the undegraded specimens did not fail up to 40% strain (indicated by the extent of necking and crazing in Figure 5). The high strain capacity was partly due to plasticisation effects of submersion and temperature as explained elsewhere [9]. Similar to the Z specimens, the degradation of F specimens resulted in a transition in the fracture mechanism from ductile to intermediate ductile-brittle and, finally, brittle failure as the plastic post-yield tail was shortened significantly by the end of 120 days. This led to a decrease in toughness, which is discussed in the next section. After 180 days of degradation, the F specimens showed a fully brittle fracture similar to that of the Z specimens, without any visible internal necking (vein-like patterns). The sideview micrographs of F specimens (Figure 5) also confirmed significant changes with respect to plastic deformation of during hydrolytic degradation. After 120 days of degradation, some degree of shear lips at the edges and internal necking could still be observed. By the end of 210 days, F specimens exhibited a smooth and flat fracture (Figure 5). It should be noted that most interesting features were identified for Z specimens and, therefore, they are the main focus here.

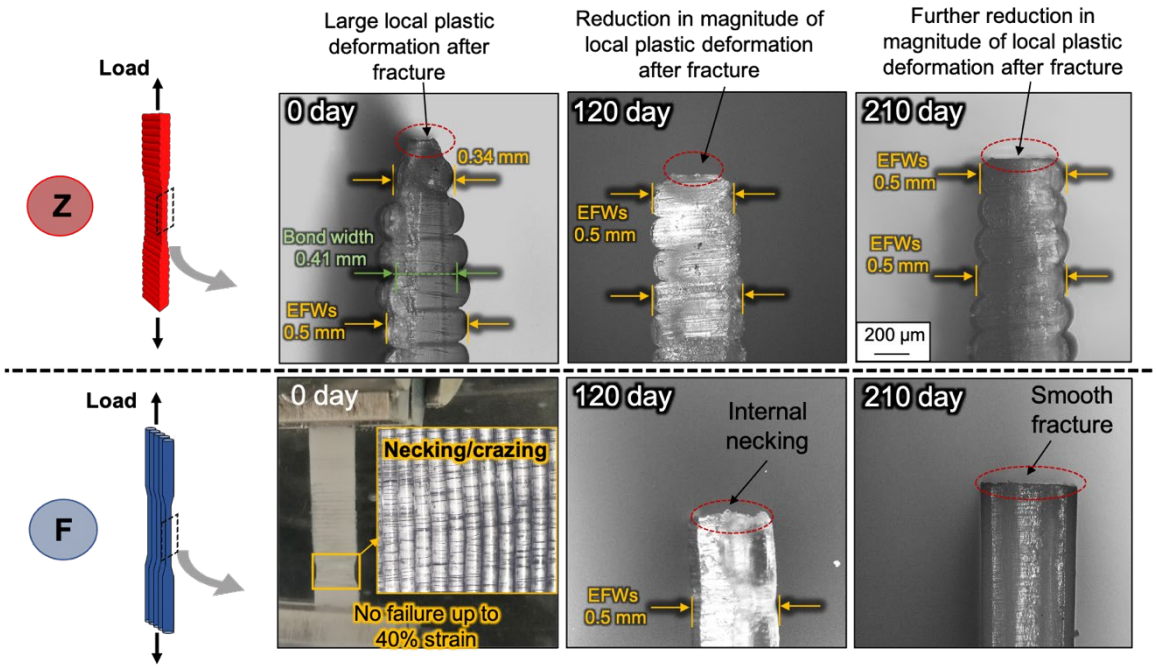

Figure 5 *Sideview micrographs of the fracture surfaces of Z (top row) and F (bottom row) specimens during degradation at 37°C showing localised plastic deformation near to, and on, the fracture surface. The length scale bar is the same for all images.*

3.2.1 Effects of molecular weight, crystallinity and mechanical properties on fracture features

Based on the observations of fracture surfaces during in vitro hydrolytic degradation in the previous section, it was decided to quantify these features in order to identify their dependencies on mechanical, chemical and thermal properties. In our previous study [11], it was demonstrated that the mechanical properties of additively manufactured PLA undergoing hydrolytic degradation initially increased with time, despite a reducing M_n through compensatory increases in degree of crystallinity. Consequently, in this study, both strain-at-fracture and toughness of Z specimens along with their fracture features were plotted as a function of M_n and crystallinity. All data were normalised by their initial values (i.e. before hydrolytic degradation).

Apparently, for normalised strain-at-fracture and toughness, a considerable reduction was found for M_n below 40 kDa (Figure 6a). This could be explained by the increase in the crystallinity (Figure 6b), which inversely affected those properties by enhancing their possibility to fragment. Both strain-at-fracture and toughness deceased by 36.5% and 42.2%, respectively, when crystallinity increased from 2.98% to 11.2% just after 60 days. Above 12% crystallinity, there was a rapid decrease in these mechanical properties, with their levels approaching zero, indicating the onset of brittle fracture as the primary mode of failure.

In the next step, the dependency of fracture features on M_n (Figure 6c) and crystallinity (Figure 6d) was considered. The brittleness remained unchanged (around 0.33) until M_n reduced below 40 kDa – after 120 days of hydrolytic degradation – and, beyond that point, brittleness accelerated towards 1 and plateaued, while distances between striations linearly decreased as M_n decreased with time. There was a cross-over point between the two fracture features at the M_n of 40 kDa – the same threshold found for strain-at-fracture and toughness – confirming that there was a critical value with respect to molecular weight.

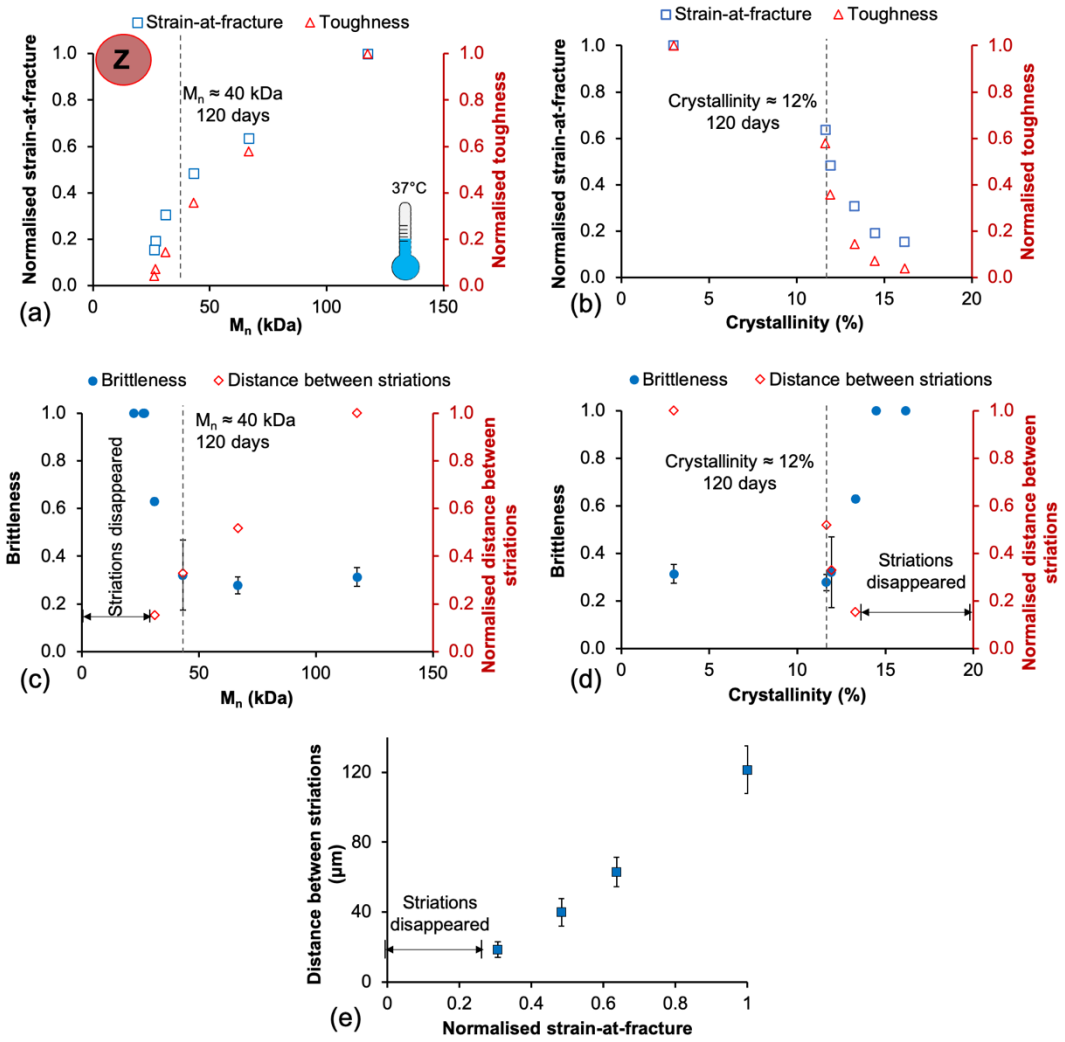

Figure 6 *Evolution of properties for Z specimens degraded at 37ºC for 240 days: normalised strain-at-fracture and toughness against M_n (a) and crystallinity (b); quantification of brittleness and normalised distance between striation against M_n (c) and crystallinity (d); (e) reduction in distance between striation as function of strain-at-fracture. Critical level of M_n - 40 kDa - and crystallinity - 12% - were found. Error bars indicate standard deviation.*

The effect of crystallinity (Figure 6d) on the fracture features was similar to that found for M_n (Figure 6c): a cross-over point between the two features was found at a crystallinity value of 12%, again similar to strain-at-fracture and toughness (Figure 6b). Beyond 12%, the material failed abruptly as indicated by saturation of the brittleness data. Finally, a linear relationship for a normalised distance between striations and M_n, similar to that of strain-at-fracture was found (Figure 6e). The reduction in M_n with time (Figure 4a) and the increase in crystallinity (Figure 4b) resulted in the reduction in distance between striations, as the material demonstrated a less ductile fracture. The effect of in vitro hydrolytic degradation was similar for the F specimens, with internal

necking features (vein-like patterns) disappearing after 120 days (indicating a transition to brittle fracture) as a result of hydrolytic degradation.

3.3 Suitability of degradation at elevated temperatures and application of results

In the literature, many studies advise the use of accelerated degradation (at elevated temperatures) to predict the lifetime of medical implants at body temperature. Therefore, the fracture mechanisms (e.g., fracture type and fracture-surface features) of F and Z specimens degraded at 50ºC and 65ºC and mechanically tested were studied and compared to the results of the previous sections. The stress-strain curves and corresponding micrographs are provided as supplementary data (See Figures S1 and S2), since the general trends with respect to changes in the slope of stress-strain curves were similar to those of at 37ºC, although at a greater rate. As anticipated, increasing the degradation temperature accelerated the rate of degradation. Mechanical properties were no longer measurable after 30 and 3 days for 50ºC and 65ºC, respectively.

Similar to 37ºC, the distance between curved striations for Z specimens reduced until they disappeared, but this transition happened at faster rates: after 10 days and 1 day for 50ºC and 65ºC, respectively. The vein-like patterns (internal necking) also disappeared for F specimens for both degradation temperatures after the same degradation times. Fracture features were analysed for Z specimens degraded at 50ºC in a manner similar to that in Section 3.2.

In terms of strain-at-fracture and toughness, a similar critical M_n of 40 kDa was identified (Figure 7a), suggesting similar mechanical behaviours of PLA at elevated temperatures. However, the cross-over point for brittleness (reducing) and distance between curved striations (increasing) against increasing M_n (Figure 7c) shifted to a higher value (around 77 kDa) compared 40 kDa for 37ºC. On the other hand, when considering strain-at-fracture and toughness against crystallinity, the same critical value of 12% was identified at the cross-over point between two parameters. Furthermore, a comparison of the evolution of brittleness and distance between striations as functions of crystallinity showed similar trends to those at 37ºC. Lastly, the magnitude of reduction in distance between striations after one day was 53.7% (50.7 μm), followed by a reduction of 16.1 μm per day until they were no longer visible – confirmation of brittle fracture (Figure 7e).

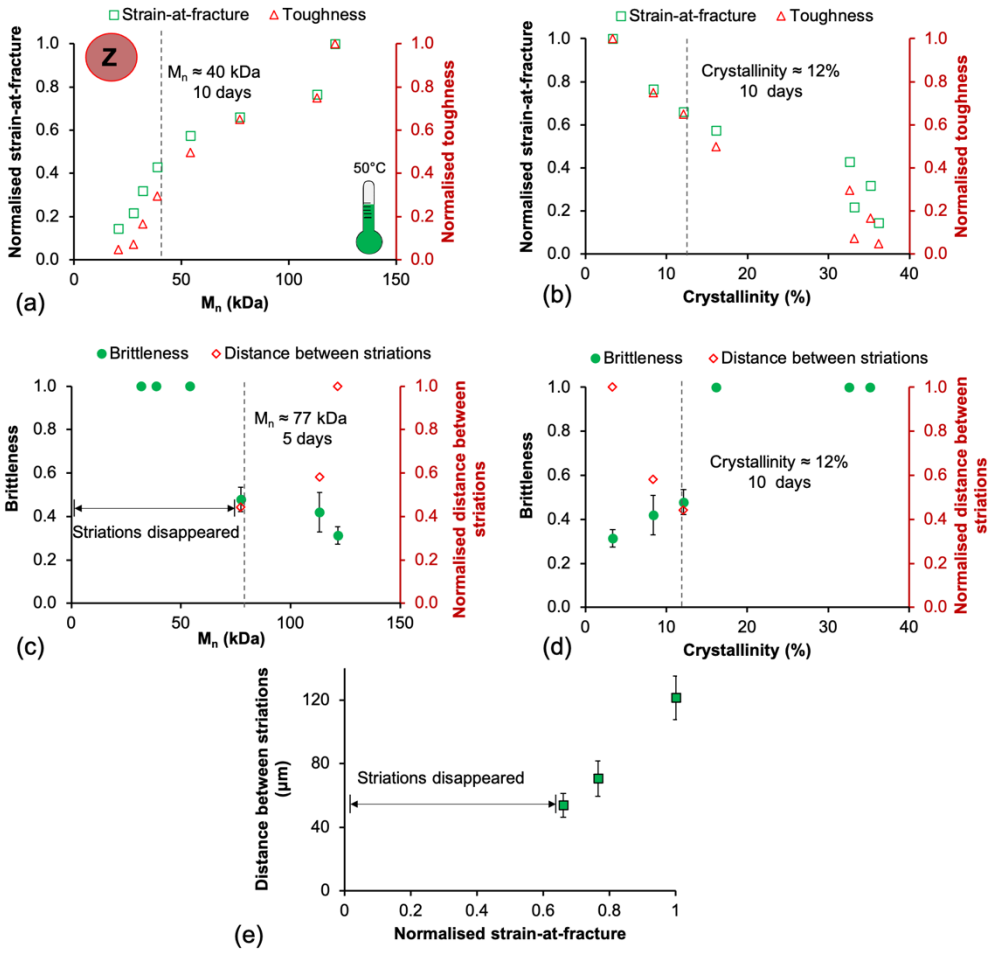

Figure 7 *Evolution of properties for Z specimens degraded at 50ºC: normalised strain-at- fracture and toughness against M_n (a) and crystallinity (b); quantification of brittleness and normalised distance between striation against M_n (c) and crystallinity (d); (e) reduction in distance between striation as function of strain-at-fracture. Critical level of crystallinity - 12% - were found similar to those that 37ºC. Error bars indicate standard deviation.*

The combined data for the brittleness parameter and the distance between striations obtained across all three temperatures were plotted against M_n (Figure 8a), crystallinity (Figure 8b) and normalised strain-at-fracture (Figure 8c) to demonstrate the potential to use elevated temperature to study the property changes at 37°C. The in vitro hydrolytic degradation temperature affected the relationship between brittleness and M_n. Brittleness approached 1 for smaller reduction in M_n at higher temperatures, which can be explained by the magnitude of change in crystallinity as a result of degradation temperature. By plotting brittleness against crystallinity, it is evident that specimens degraded at all three temperatures showed a similar trend in terms of evolution of brittleness with respect to crystallinity, by demonstrating a rapid

increase in the parameter once crystallinity increased beyond 12% (Figure 8b). Lastly, the evolution of the distance between striations with respect to strain-at-fracture also exhibited similar trends for 37ºC and 50ºC (Figure 8c; too few data points were obtained for 65°C for inclusion in this plot), indicating that accelerated tests may be suitable for prediction of fracture mechanisms during its hydrolytic degradation.

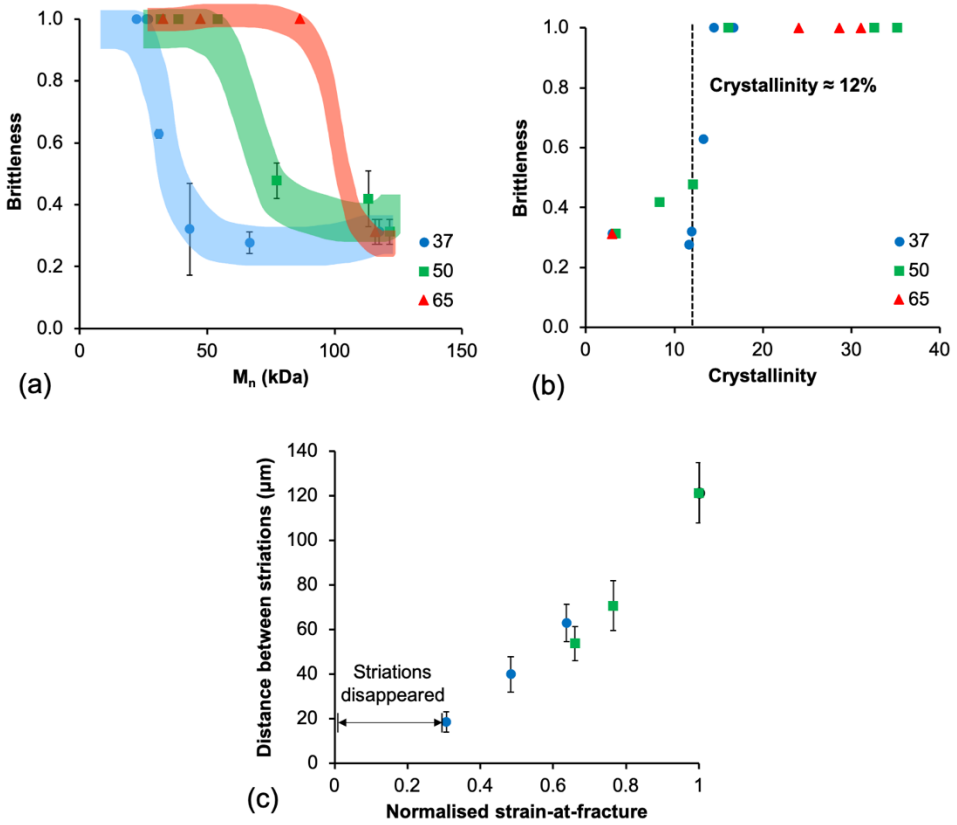

Figure 8 *Evolution of brittleness against M_n (a), crystallinity (b) and distance between striations (c) against normalised strain-at-fracture for all three temperatures. The increase in brittleness as a function of M_n showed the dependency of data on degradation temperature. Brittleness approached 1 when crystallinity was more than 12%. Error bars indicate standard deviation.*

The findings of this study may be useful for a range of applications including biomedical ones, where additively manufactured PLA parts are exposed to different environments than those found in laboratory. For example, for bioresorbable stents, it is important to ensure that the mechanical behaviour of a polymeric implant is well understood for different timescales to prevent any catastrophic failures. Ideally, stents should have high plasticity before failure to withstand the deformation from the deployment. The findings of this study may help to understand the plastic behaviour of stents in terms of the transition from ductile to brittle behaviour during hydrolytic degradation. The new understanding developed in this study was only possible by

employing a simple yet novel design of test specimens to characterise the fracture surface as opposed to using ASTM specimens with non-standardised and complex print paths. The breadth of this study was only achievable because this specimen design allowed us to produce 476 specimens for degradation analysis, which would have been impossible with ASTM D638 standard design. This number of specimens used less than 200 g polymer in total and approximately 14 hours of printing.

4 Conclusions

In this study, for the first time the role of in vitro hydrolytic degradation on fracture mechanisms of additively manufactured polylactide for biomedical applications was investigated. To improve the confidence in results, specimens were tested submerged at 37ºC to replicate human body conditions. Changes in fracture behaviour of bulk polymer and the interface bonds between layers during hydrolytic degradation at 37ºC were evaluated, identifying significant qualitative and quantitative changes of the fracture surfaces. For example, in interfacial specimens, curved striations (an indication of ductility) were observed but the distance between them decreased as degradation proceeded, indicating a transition to brittle behaviour. Similarly, for bulk polymer, the extensive localised necking reduced until a flat brittle fracture surface was apparent at advanced stages of hydrolytic degradation. Quantitative analyses of fracture features of interfacial specimens with respect to changes in crystallinity, which increased during degradation, indicated that beyond a critical value of 12% crystallinity, specimens rapidly transitioned from ductile fracture to brittle one. Furthermore, the suitability of accelerated temperatures (50ºC and 65ºC) to predict the Fracture mechanism of specimens at body temperature was evaluated. The results of this study clearly demonstrate the benefit of using an appropriate testing design to allow developing a new understanding of fracture mechanisms of 3D-printed PLA, which can be useful for design of medical implants that could undergo hydrolytic degradation.

Acknowledgements

This research did not receive any specific grant from funding agencies in the public, commercial, or not-for-profit sectors.

Appendix A. Supplementary data

The representative stress-strain curves along with optical micrographs of fracture surfaces for Z and F specimens degraded at 50ºC and 65ºC are shown in Figures S1 and S2, respectively.

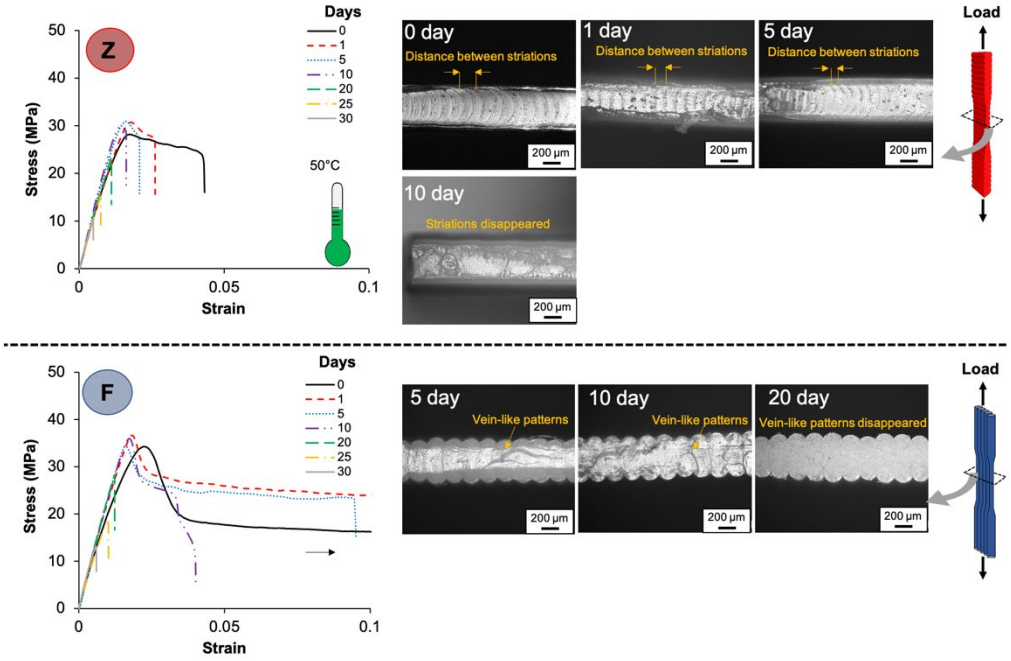

Figure S1 *Representative stress-strain curves along with optical micrographs of fracture surfaces for Z and F specimens degraded at 50ºC.*

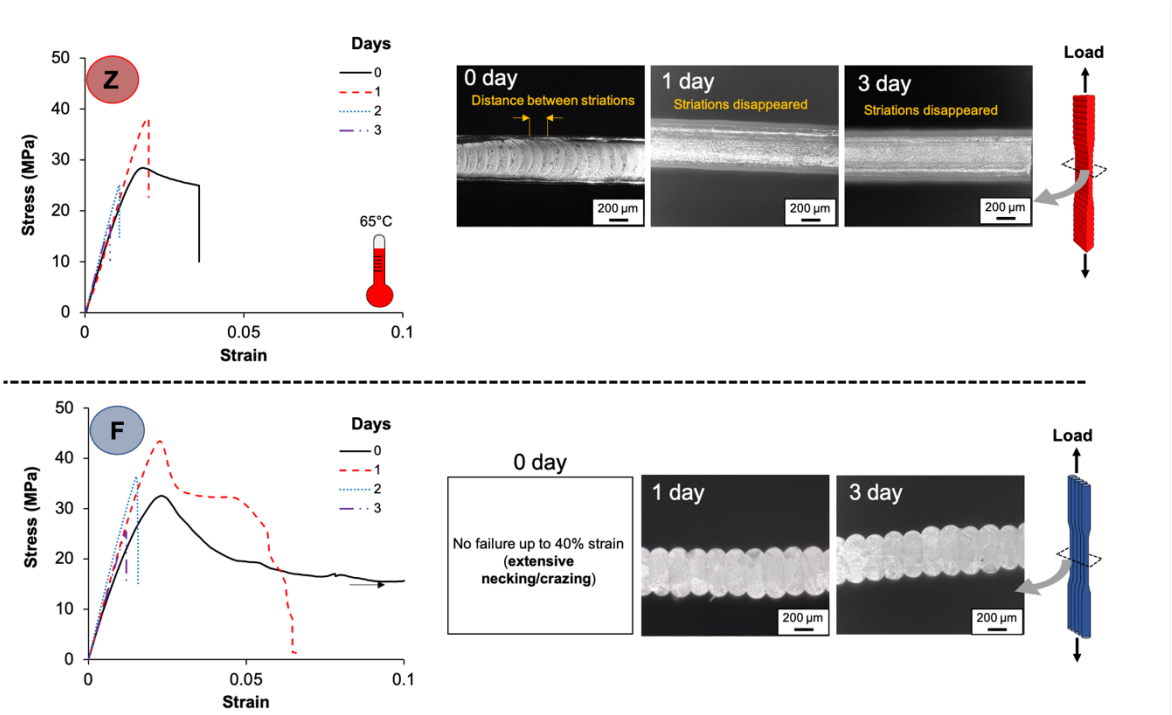

Figure S2 *Representative stress-strain curves along with optical micrographs of fracture surfaces for Z and F specimens degraded at 65ºC.*

References

[1] L. S. Nair and C. T. Laurencin, "Biodegradable polymers as biomaterials," *Prog. Polym. Sci.*, vol. 32, no. 8–9, pp. 762–798, 2007.

[2] D. Da Silva *et al.*, "Biocompatibility, biodegradation and excretion of polylactic acid (PLA) in medical implants and theranostic systems," *Chem. Eng. J.*, vol. 340, pp. 9–14, 2018.

[3] S. Farah, D. G. Anderson, and R. Langer, "Physical and mechanical properties of PLA, and their functions in widespread applications — A comprehensive review," *Adv. Drug Deliv. Rev.*, vol. 107, pp. 367–392, 2016.

[4] H. Xu, X. Yang, L. Xie, and M. Hakkarainen, "Conformational footprint in hydrolysis-induced nanofibrillation and crystallization of poly(lactic acid)," *Biomacromolecules*, vol. 17, no. 3, pp. 985–995, 2016.

[5] A. Gleadall, D. Visscher, J. Yang, D. Thomas, and J. Segal, "Review of additive manufactured tissue engineering scaffolds: relationship between geometry and performance," *Burn. Trauma*, vol. 6, pp. 1–16, 2018.

[6] C. Culmone, G. Smit, and P. Breedveld, "Additive manufacturing of medical instruments: A state-of-the-art review," *Addit. Manuf.*, vol. 27, no. March, pp. 461–473, 2019.

[7] M. A. Elsawy, K. H. Kim, J. W. Park, and A. Deep, "Hydrolytic degradation of polylactic acid (PLA) and its composites," *Renew. Sustain. Energy Rev.*, vol. 79, pp. 1346–1352, 2017.

[8] L. Safai, J. S. Cuellar, G. Smit, and A. A. Zadpoor, "A review of the fatigue behavior of 3D printed polymers," *Addit. Manuf.*, vol. 28, pp. 87–97, 2019.

[9] A. Moetazedian, A. Gleadall, X. Han, and V. V. Silberschmidt, "Effect of environment on mechanical properties of 3D printed polylactide for biomedical

applications," *J. Mech. Behav. Biomed. Mater.*, vol. 102, p. 103510, 2020.
[10] J. Allum, A. Moetazedian, A. Gleadall, and V. V. Silberschmidt, "Interlayer bonding has bulk-material strength in extrusion additive manufacturing: New understanding of anisotropy," *Addit. Manuf.*, vol. 34, p. 101297, Aug. 2020.
[11] A. Moetazedian, A. Gleadall, X. Han, A. Ekinci, E. Mele, and V. V. Silberschmidt, "Mechanical performance of 3D printed polylactide during degradation," *Addit. Manuf.*, p. 101764, 2020.
[12] J. Gonzalez Ausejo *et al.*, "A comparative study of three-dimensional printing directions: The degradation and toxicological profile of a PLA/PHA blend," *Polym. Degrad. Stab.*, vol. 152, pp. 191–207, 2018.
[13] J. Allum, A. Gleadall, and V. V. Silberschmidt, "Fracture of 3D-printed polymers: Crucial role of filament-scale geometric features," *Eng. Fract. Mech.*, vol. 224, p. 106818, 2020.
[14] A. Moetazedian, A. S. Budisuharto, V. V. Silberschmidt, and A. Gleadall, "CONVEX (CONtinuously Varied EXtrusion): a new scale of design for additive manufacturing," *Addit. Manuf.*, p. 101576, 2020.
[15] ASTM D1708-18, "Standard Test Method for Tensile Properties of Plastics By Use of Microtensile," 2002.
[16] ISO, "Implant for surgery-Homopolymers, copolymers and blends on poly(lactide)- In vitro degradation testing," 2017.
[17] O. Vyavahare, D. Ng, and S. L. Hsu, "Analysis of structural rearrangements of poly(lactic acid) in the presence of water," *J. Phys. Chem. B*, vol. 118, no. 15, pp. 4185–4193, 2014.
[18] R. Naseem *et al.*, "Mechanical and chemical characterisation of bioresorbable polymeric stent over two-year in vitro degradation," *J. Biomater. Appl.*, vol. 34, no. 1, pp. 61–73, 2019.
[19] R. M. Felfel, K. M. Z. Hossain, A. J. Parsons, C. D. Rudd, and I. Ahmed, "Accelerated in vitro degradation properties of polylactic acid/phosphate glass fibre composites," *J. Mater. Sci.*, vol. 50, no. 11, pp. 3942–3955, 2015.
[20] M. J. Doyle, A. Maranci, E. Orowan, and S. T. Stork, "The Fracture of Glassy Polymers," *Proc. R. Soc. Lond. A.*, vol. 329, no. 1577, pp. 137–151, 1972.
[21] A. Moetazedian, A. Gleadall, E. Mele, and V. V Silberschmidt, "Damage in extrusion additive manufactured parts : effect of environment and cyclic loading," *Procedia Struct. Integr.*, vol. 28, pp. 452–457, 2020.